

**The Sidi Ifni transect across the rifted margin of Morocco (Central Atlantic)
Vertical movements constrained by low-temperature thermochronology**

Charton, Rémi; Bertotti, Giovanni; Arantegui, Angel; Bulot, Luc

DOI

[10.1016/j.jafrearsci.2018.01.006](https://doi.org/10.1016/j.jafrearsci.2018.01.006)

Publication date

2018

Document Version

Accepted author manuscript

Published in

Journal of African Earth Sciences

Citation (APA)

Charton, R., Bertotti, G., Arantegui, A., & Bulot, L. (2018). The Sidi Ifni transect across the rifted margin of Morocco (Central Atlantic): Vertical movements constrained by low-temperature thermochronology. *Journal of African Earth Sciences*, 141, 22-32. <https://doi.org/10.1016/j.jafrearsci.2018.01.006>

Important note

To cite this publication, please use the final published version (if applicable).
Please check the document version above.

Copyright

Other than for strictly personal use, it is not permitted to download, forward or distribute the text or part of it, without the consent of the author(s) and/or copyright holder(s), unless the work is under an open content license such as Creative Commons.

Takedown policy

Please contact us and provide details if you believe this document breaches copyrights.
We will remove access to the work immediately and investigate your claim.

1 **Title**

2 The Sidi Ifni transect across the rifted margin of Morocco (Central Atlantic): Vertical
3 movements constrained by low-temperature thermochronology.

4 **Authors and Affiliations**

5 **Rémi Charton**, Department of Geoscience and Engineering, Delft University of
6 Technology, P.O. Box 5048, 2600 GA Delft, The Netherlands

7 Corresponding author

8 r.j.g.charton@tudelft.nl

9 +31(0)152787958

10 **Giovanni Bertotti**, Department of Geoscience and Engineering, Delft University of
11 Technology, P.O. Box 5048, 2600 GA Delft, The Netherlands

12 g.bertotti@tudelft.nl

13 **Angel Arantegui**, School of Earth and Environmental Sciences, The University of
14 Manchester, M13 9PL Manchester, United Kingdom

15 angel.arantegui@manchester.ac.uk

16 **Luc Bulot**, UM 34 Cerege CNRS (UMR 7630) – IRD (UMR 161), Aix–Marseille Université
17 (Centre Saint-Charles), Place Victor Hugo, 13331 Marseille cedex 03, France

18 bulot@cerege.fr

19 &

20 NARG

21 luc.bulot@manchester.ac.uk

22

23 **All authors:** NARG (North Africa Research Group), UK

24
25
26
27
28
29
30
31
32
33
34
35

36

37

38
39
40
41
42

Abstract

The occurrence of km-scale exhumations during syn- and post-rift stages has been documented along Atlantic continental margins, which are also characterised by basins undergoing substantial subsidence. The relationship between the exhuming and subsiding domains is poorly understood. In this study, we reconstruct the evolution of a 50 km long transect across the Moroccan rifted margin from the western Anti-Atlas to the Atlantic basin offshore the city of Sidi Ifni. Low-temperature thermochronology data from the Sidi Ifni area document a ca. 8 km exhumation between the Permian and the Early/Middle Jurassic. The related erosion fed sediments to the subsiding Mesozoic basin to the NW. Basement rocks along the transect were subsequently buried by 1 to 2 km between the Late Jurassic and the Early Cretaceous. From late Early/Late Cretaceous onwards, rocks present along the transect were exhumed to their present-day position.

Keywords

Sidi Ifni transect, Morocco, Central Atlantic, Vertical movements

Highlights

- Post-Variscan exhumation of the Anti-Atlas ceased during the Early/Middle Jurassic.
- Exhumation resumed during the Late Cretaceous.
- A period of subsidence is observed during the Late Jurassic to Early Cretaceous.
- The rifted Moroccan margin records variable post-Variscan thermal history along strike.

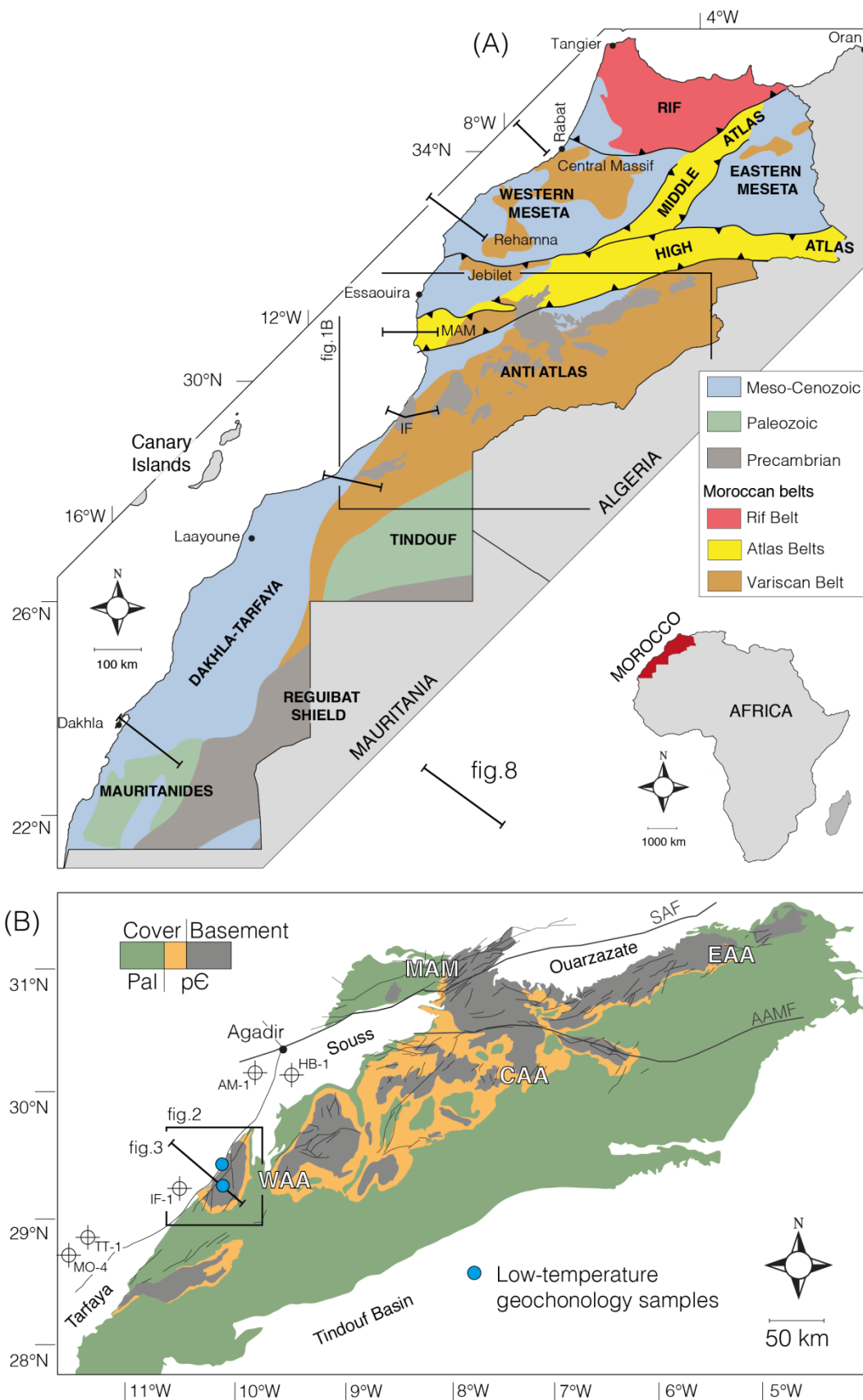
43

1. Introduction

44 The models of passive margin evolution (reviewed in Watts, 2012) have been questioned
45 in the last decade. Recent studies have convincingly documented the occurrence of
46 episodic km-scale exhumations and subsidences during the syn- and post-rift stages of
47 rifted margin evolution (e.g. Japsen *et al.*, 2016) .

48 Syn-rift upward movements are common in Atlantic continental margins (e.g. Oukassou *et al.*,
49 2013; Jelinek *et al.*, 2014; Japsen *et al.*, 2016) and have usually been attributed to rift
50 shoulder uplift. Post-rift upward movements have been documented along the North (e.g.
51 Japsen *et al.*, 2006; Japsen *et al.*, 2016), Central (e.g. Bertotti and Gouiza, 2012; Amidon
52 *et al.*, 2016) and South (e.g. Jelinek *et al.*, 2014; Wildman *et al.*, 2015) Atlantic margins.
53 Beyond the Atlantic realm, Australian margins have experienced similar movements (e.g.
54 Tassone *et al.*, 2012). As several studies in Morocco have proposed (e.g. Bertotti and
55 Gouiza, 2012), anomalous vertical movements in the exhuming domain are coeval to
56 excessive downward movements in the subsiding domain.

57 Despite the well-established body of evidence supporting syn- and post-rift exhumations,
58 we still lack a quantitative comprehension of these movements. The proposed numerical
59 models (e.g. Yamato *et al.*, 2013) are fairly general and still unable to provide predictions
60 by which they can be tested against observations from natural systems. This is partly due
61 to the fact that most of these enigmatic vertical movements are documented onshore using
62 Low-Temperature Thermochronology (LTT), without any attempt to link them to the
63 movements in offshore areas. These observations call for an integrated analysis of the
64 entire system from the exhuming domain (source) to the subsiding region (sink) as a
65 required step to fully understand the involved tectonics.



66

67 Figure 1. A) Simplified structural map of Morocco (after Hollard *et al.* 1985). B) Simplified
 68 geological map of the Anti-Atlas (after Hollard *et al.*, 1985; Soulaïmani *et al.*, 2014) with sample
 69 locations. MAM: Massif Ancien de Marrakech; IF: Sidi Ifni area; WAA, CAA, and EAA: Western,
 70 Central, and Eastern Anti-Atlas, respectively; Pal: Palaeozoic; pC: Precambrian.

71 In this study, we construct a 50 km long transect across the Moroccan rifted margin (fig.
72 **1A**) from the western Anti-Atlas to the offshore passive margin basin (fig. **1B**), that we call
73 the Sidi Ifni transect. The coexistence of Mesozoic sediments and regional unconformities
74 in the study area makes it a key transition between the generally subsiding offshore and
75 exhuming Anti-Atlas (e.g. Gouiza *et al.*, 2017). Expanding the presently available low-
76 temperature geochronology data base and using new and robust stratigraphic ages of the
77 Mesozoic sediments, we present a reconstruction of syn- and post-rift vertical movements
78 along the Sidi Ifni transect. We also compare the present-day structure and evolution of
79 the Sidi Ifni transect to those of other segments across the Moroccan rifted margin,
80 namely, the Rabat, Doukkala, Essaouira, North-Tarfaya and Dahkla transects.

81

2. Geological setting

82 The WSW/ENE oriented Anti-Atlas (fig. 1) extends over 600 km with elevations reaching
83 3305 m towards its centre. The basement of the belt is composed of Neoproterozoic
84 granites and metamorphic rocks (Pan-African orogeny ; e.g. Thomas *et al.*, 2004). The
85 Anti-Atlas basement is partially covered by autochthonous Late Neoproterozoic and
86 Palaeozoic sediments (e.g. Michard *et al.*, 2008b). These rocks were deformed during the
87 late Palaeozoic Variscan orogeny, which is characterised by a strong inversion and thick-
88 skin folding (e.g. Burkhard *et al.*, 2006). The presently outcropping Precambrian inliers (fig.
89 **1B**) are basement folds that formed during the Variscan deformation (*plis de fond*; e.g.
90 Helg *et al.*, 2004).

91 The rifting of the Central Atlantic started in the Late Triassic and ended in the Early to
92 Middle Jurassic (e.g. Michard *et al.*, 2008a; Labails *et al.*, 2010), and led to the separation
93 of the Central Atlantic passive margins. The convergence between the African and
94 European plates started in the Late Cretaceous, resulting from the South Atlantic opening
95 (Piqué *et al.*, 2002). In North-West Africa, the Cenozoic is marked by the Atlas orogeny.
96 The collision between the European and African tectonic plates and related deformations
97 that occurred in the Eocene onwards (reviewed in Frizon de Lamotte *et al.*, 2009), are
98 considered as mild with long wavelength crustal folding in the Anti-Atlas.

99 3. Present-day architecture of the Sidi Ifni transect

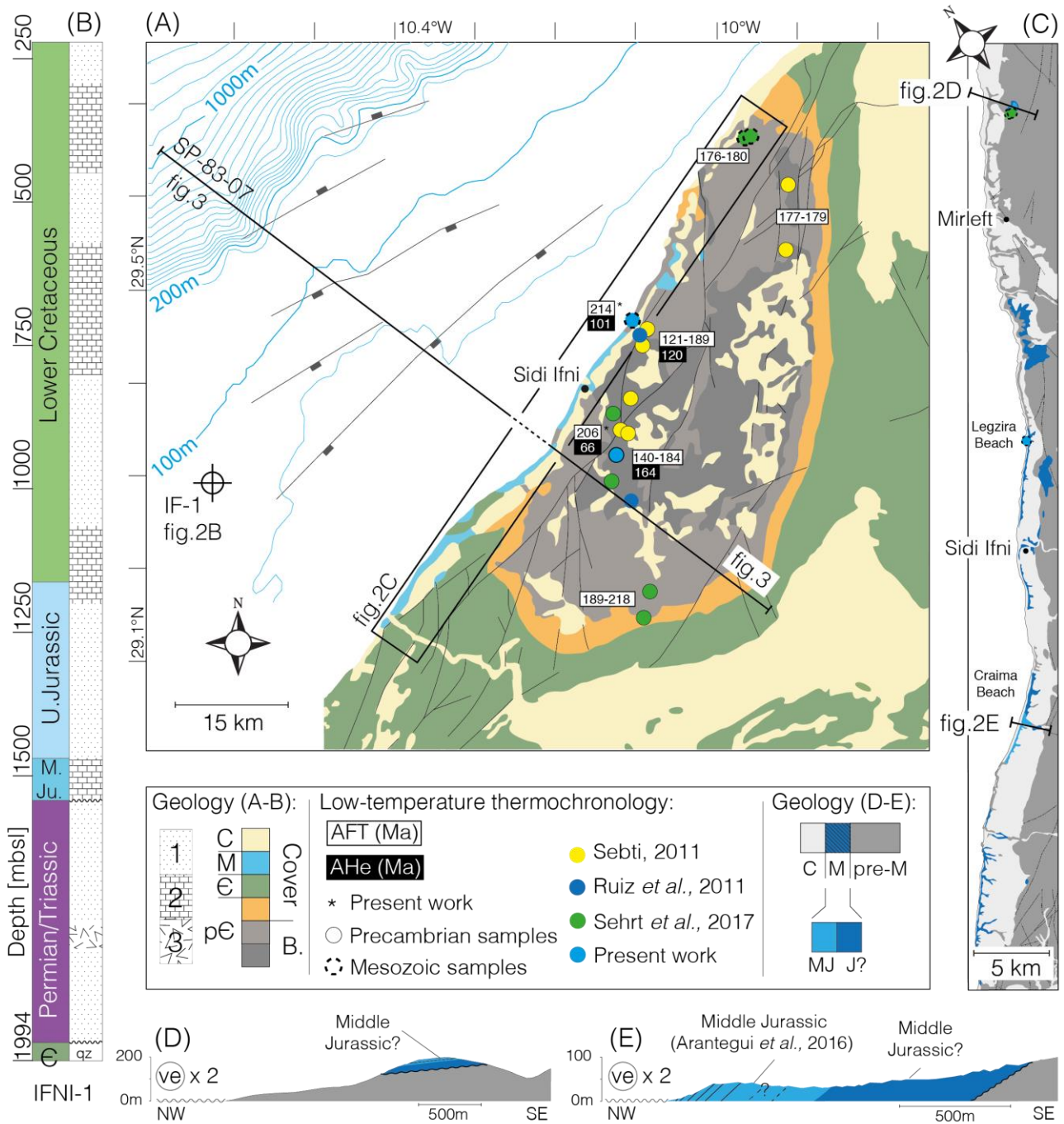
100 The Sidi Ifni transect (figs. 2 and 3) is composed of the Sidi Ifni dome in the onshore
101 domain and of the Atlantic continental shelf, slope, and abyssal basin in the offshore
102 domain. The pre-Mesozoic basement outcropping onshore is affected offshore by NW and
103 SE dipping normal faults, which bound syn-rift half grabens.

104 On the continental shelf, the Ifni-1 well shows ca. 2 km thick Mesozoic sediments (fig. 2B),
105 comprising the syn- and post-rift packages. The syn-rift Permian?-Triassic sediments are
106 truncated by the Middle Jurassic sediments close to the shoreline. Westwards, Lower
107 Jurassic platform sediments thin into basinal facies (Hafid *et al*, 2008), while they are
108 truncated near the coast, and are missing in Ifni-1 well. The latter shows a Middle Jurassic
109 section of mixed carbonates and clastics.

110 Mesozoic sediments in contact with Palaeozoic and Precambrian rocks are exposed along
111 a narrow NE-SW oriented domain along the coastline (fig. 2B). Intertidal fine clastics and
112 shallow marine carbonates, previously mapped as Lower Cretaceous or pre-Cenomanian
113 (Hollard *et al.*, 1985; Yazidi *et al.*, 1986; 1991), have been re-dated using benthic
114 foraminifera, green algae, gastropods and bivalves as Middle Jurassic (fig. 2D; Arantegui
115 *et al.*, 2016; see appendix). Underlying undated sediments stratigraphically conformable
116 are fluvial clastics (figs. 2C and 2E), and will be considered in this work as Middle Jurassic.
117 Based on field observations, their architecture shows alluvial fans downlapping on
118 basement rocks laterally associated to alluvial plain deposits.

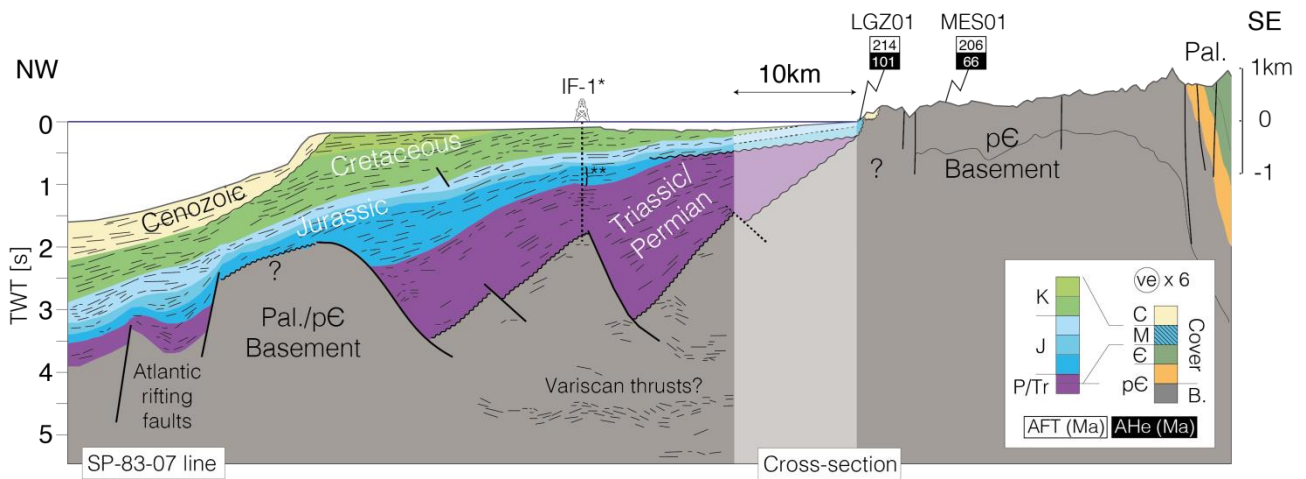
119 Offshore, undifferentiated Upper Jurassic/Lower Cretaceous neritic clastics overly the
120 Upper Jurassic carbonate platform, and are referred to as the 'Sables de Tan-Tan'
121 Formation (e.g. Choubert *et al.*, 1966; Martinis and Visintin, 1966). Finally, the Lower
122 Cretaceous reflections in line SP-83-07 are interpreted as up-dip truncations close to the
123 seabed in the continental shelf domain. The Cretaceous sediments drilled in Ifni-1 are
124 neritic clastics and carbonates. The Middle Cretaceous (Aptian-Albian) to Cenozoic

125 sediments are only preserved close to the shelf edge and further offshore, while the Late
126 Cretaceous sediments are not recorded in the study areas.



127

128 Figure 2. A) Simplified geological map of the Sidi Ifni area (after Hollard *et al.*, 1985) and low-
 129 temperature thermochronology data locations (Sebti, 2011; Ruiz *et al.*, 2011; Sehrt *et al.*, 2017;
 130 present study). Bathymetry contour lines are every 50 m. Syn-rift offshore normal faults are from
 131 Le Roy and Piqué (2001). C: Cenozoic; M: Mesozoic; E: Cambrian; pE: Precambrian; AFT: Apatite
 132 fission track ages; AHe: (U-Th)/He dating on apatites. B) Stratigraphic log of the Ifni-1 (IF-1) well
 133 (after well report; 70 to 222 mbsl were not examined). 1: Neritic clastics and sandstones
 134 (continental for the Triassic), 2: limestones/dolomites, 3: evaporites. C) Simplified geological map
 135 of the Sidi Ifni Margin with highlight on Mesozoic sediments (after 1/100000 geological maps of
 136 Tiznit and Sidi Ifni; Yazidi *et al.*, 1986; 1991). J?: Middle Jurassic fluvial red conglomerates and
 137 red/pink/grey coarse to very coarse sandstones; MJ: Intertidal fine clastics and shallow marine
 138 carbonates identified as Middle Jurassic (Arantegui *et al.*, 2016; see appendix). D-E) Cross-
 139 sections illustrating the geometry of the contact between the Sidi Ifni basement rocks and the
 140 Mesozoic sediments.



141

142 Figure 3. The Sidi Ifni transect: composite cross-section running through the Sidi Ifni area,
 143 based on the interpretation of the 2D seismic line SP-83-07 from Gouiza (2011) and from the
 144 geological map from Hollard *et al.* (1985). The seismic line ends ca. 10 km before the shoreline.
 145 The gap (dashed line in figure 2A) was interpolated from the seismic interpretation and the
 146 geological map; the LTT ages are projected. IF-1 is projected on the basement high (*) at 2 second
 147 (TWT). The well report does not document traversing Lower Jurassic sediments but only Triassic
 148 and Middle Jurassic (**). Lower Jurassic sediments are present on the seismic section at the well
 149 projection position, but are truncated less than 10 km to the SE. C: Cenozoic; M: Mesozoic (K:
 150 Cretaceous; J: Jurassic; Tr: Triassic); P: Permian; E: Cambrian; pE: Precambrian.

151 **4. LTT and t-T modeling: Methods and results**

152 The samples MES01 and LGZ01 were collected from a granite of the Precambrian
153 basement and the Middle Jurassic conglomerate of Lgezira beach, respectively (fig. 4).
154 Apatite crystals within these samples were analysed for apatite fission tracks (AFT) and
155 (U-Th)/He (AHe). The AFT measurements (table 1) were carried-out at Dalhousie
156 University (Halifax, Canada) by B.Louis, and ages were calculated using the external
157 Detector method (Gallagher *et al.*, 1998). The method is described in Louis (2015). The
158 AHe analyses were conducted in Dalhousie University (Halifax, Canada) by R.Kislitsyn,
159 based on K.Farley's technique summarized in Farley (2002).

160
161 The two samples produced Triassic AFT ages (206.1 ± 10.3 and 214.3 ± 8.8 Ma) and
162 Cretaceous reproducible AHe ages (66.6 ± 4 and 100.7 ± 6 Ma). The abundance of confined
163 tracks between 12-14 μm (fig. 4) is the results of long residence above the Apatite Partial
164 Annealing Zone (APAZ; Bigot-Cormier, 2002) and is compatible with rapid cooling through
165 the APAZ (e.g. Ghorbal *et al.*, 2008). The dispersion of AHe single grain ages suggests a
166 partial opening of the He system (Rougier *et al.*, 2013) between ca.170 and 60 Ma for
167 MES01 and between 140 and 50 Ma for LGZ01.

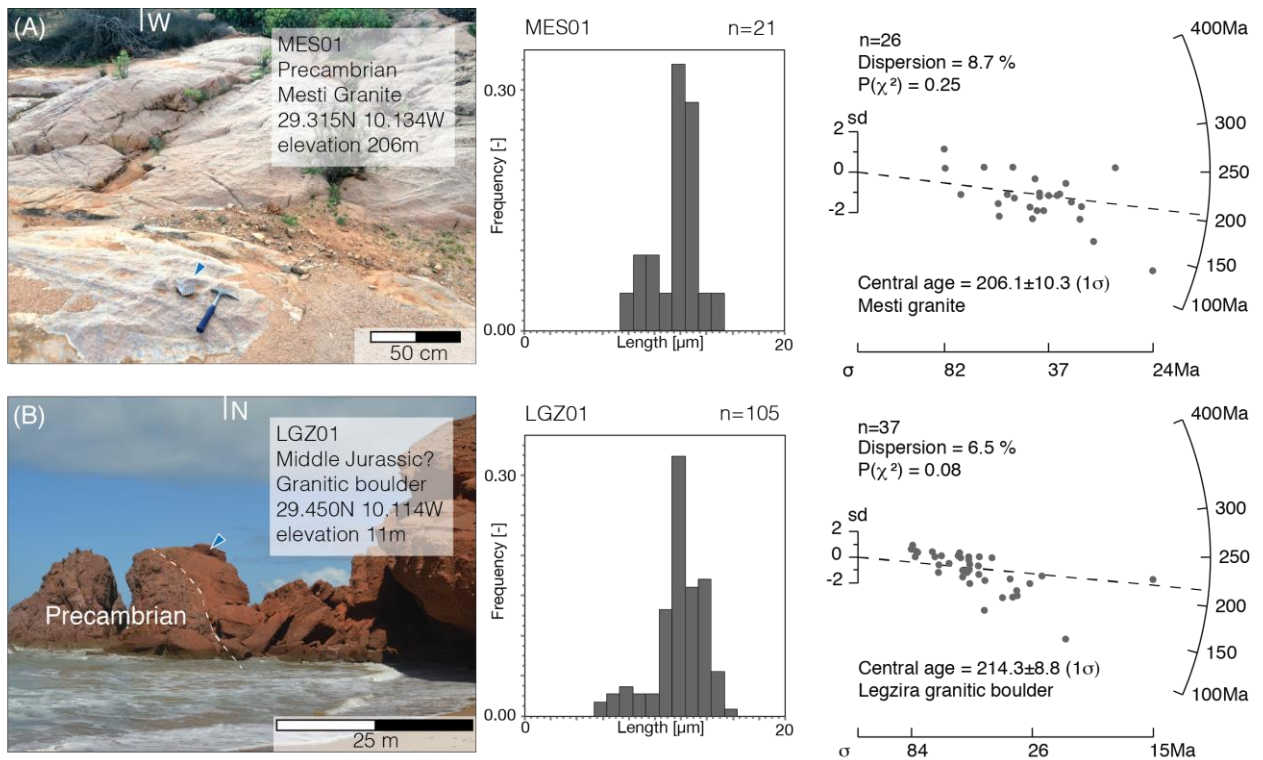
Samples	n	U [ppm]	ρ_s [$\times 10^5$ tr cm ⁻²] (n_s)	ρ_i [$\times 10^5$ tr cm ⁻²] (n_i)	ρ_d [$\times 10^5$ tr cm ⁻²] (n_d)	P(χ^2) %	AFT Ages $\pm 1\sigma$ [Ma]	MTL $\pm 1\sigma$ [μ m]	Std _{MTL} [μ m]	n_{TL}	Dpar [μ m]	Std _{Dpar} [μ m]
MES01	26	25.1	2.24 (1430)	2.19 (1399)	11.4 (6234)	25.1	206.07 \pm 10.29	11.38 \pm 0.85	1.93	21	2.23	0.82
LGZ01	36	32.9	2.933 (2518)	2.86 (2455)	11.8 (6234)	8.5	214.27 \pm 8.85	11.77 \pm 0.31	1.98	105	2.3	0.92

168 Table 1. Apatite Fission track results. n is the number of analyzed apatite crystals. ρ_s is the
169 density of spontaneous tracks, ρ_i is the density of induced tracks, and ρ_d is the density of fossil
170 tracks. n_s , n_i , and n_d are the amount of tracks used for the density calculation. P(χ^2)% is the Chi-
171 square probability; samples pass the Chi-square test when P>5%. AFT ages are central ages with
172 error $\pm 1\sigma$. MTL is the mean track lengths with error $\pm 1\sigma$ and standard deviation Sdt_{MTL}. n_{TL} is the
173 number of measured track lengths. Dpar is the diameter of etched spontaneous tracks measured
174 parallel to the c-axis and is associated to its standard deviation Std_{Dpar}. Zeta (ζ)=362.3 is the
175 correcting factor defined by Fleischer and Hart (1972); $\sigma(\zeta)$ =8.6 is the zeta uncertainty (Traditional
176 calibration; Hurford, 1990).

Sample Aliquots	U [ppm]	Th [ppm]	¹⁴⁷ Sm [ppm]	Th/U	eU [ppm]	He [fmol]	Radius [μm]	Mass [μg]	Uncorrected He age±1σ [Ma]	Ft factor	Corrected He age±1σ [Ma]
MES01_I	21.8	33.1	13.3	1.5	29.5	21.9	40.5	1.9	73.0±4.4	0.65	113.0±6.8
MES01_II	18.9	29.0	9.5	1.5	25.6	30.8	54.0	4.5	48.5±2.9	0.73	66.6±4.0
MES01_III	15.0	24.5	8.5	1.6	20.7	11.8	42.0	2.0	52.0±3.1	0.65	79.7±4.8
MES01_IV	19.5	24.7	9.5	1.3	25.2	64.5	52.0	3.7	124.5±7.5	0.72	172.6±10.4
MES01_V	21.1	34.1	12.6	1.6	29.0	6.8	35.0	1.0	40.8±2.5	0.59	69.2±4.2
MES01 Mean	20.0	31.5	11.0				44.5				100.2±6.0
LGZ01_I	24.2	27.1	27.4	1.1	30.6	25.5	44.0	2.6	58.9±3.5	0.68	87.0±5.2
LGZ01_II	46.9	59.4	43.6	1.3	60.8	34.5	40.0	1.6	64.4±3.9	0.64	100.7±6.0
LGZ01_III	32.5	55.6	30.7	1.7	45.4	74.2	45.5	3.1	96.0±5.8	0.68	140.5±8.4
LGZ01_IV	24.8	27.0	24.5	1.1	31.1	85.2	57.0	5.9	84.8±5.1	0.75	113.5±6.8
LGZ01_V	21.0	30.0	26.9	1.4	28.0	11.5	41.0	2.3	33.2±2	0.65	51.1±3.1
LGZ01 Mean	29.9	39.8	30.6				45.5				98.6±5.9

177
178
179
180

Table 2. Result of apatite (U-Th)/He analyses. Five aliquots from each sample were analyzed. AHe ages are corrected using the Ft factor based on crystal geometries. **eU**: effective uranium. Mean concentrations, radius, and ages are used as input in t-T modelling.



181
 182 Figure 4. Sampled outcrops (left panel), track length distribution (central panel), and radial
 183 plots (bivariate scatterplots; right panel). A) Precambrian granite of the Sidi Ifni area exposed in a
 184 riverbed close to the city of Mesti, where MES01 was sampled. B) Middle Jurassic red beds (or
 185 older; Arantegui *et al.*, 2016; see appendix) lying unconformably on the Proterozoic basement,
 186 located north of the Lgzira village, and where LGZ01 was sampled. Radial plots were made with
 187 RadialPlotter with Linear Transformation (Vermeesch, 2009). sd: standard deviation; σ : error with
 188 1σ (Ma) (with precision given by $1/\sigma$); χ^2 : Chi-square probability.

189 Time-Temperature (t-T) paths were obtained by modelling AFT lengths, Dpar, and
190 AFT/AHe ages with the inverse modelling HeFTy software (Ketcham, 2005; table 3 and fig.
191 5). HeFTy runs a Monte Carlo algorithm that generates time-temperature paths that match
192 to a certain extent (Goodness Of Fit, GOF) the input data. In the present study we use
193 AFT models (composed of the AFT single-grain age data and the confined track lengths)
194 and AHe models (composed of the mean AHe corrected age, the chemical composition,
195 and radius of the apatite crystal). Paths are considered 'acceptable' when the GOF for the
196 AFT model is between 5 and 50%, and 'good' when higher than 50%. The 'best fit' path
197 has the highest GOF for both AHe and AFT models.

198 Five constraints are imposed in this study. Constraint 'a' (300-260°C/300-295 Ma) is based
199 on the end of the Palaeozoic low-grade metamorphism documented by Ruiz *et al.* (2008)
200 in the western Anti-Atlas (note that the authors described it from 330 to 300 Ma, which is
201 on the edge of our modelling window)

202 Constraint 'b' (200-160 Ma) is based on the Jurassic sediments lying on Palaeozoic and
203 Precambrian rocks in the onshore Sidi Ifni area (Arantegui *et al.*, 2016; see appendix).
204 Importantly, the constraint is set at surface temperature for the granitic boulder (30-10°C),
205 and close to surface temperatures for the sampled granite (60-20°C). Indeed, the later
206 must have been protected from Jurassic erosion by the Precambrian (and Palaeozoic?)
207 rock column sitting on top of it. Constraint 'c' (110-50°C/AHe age \pm 10 Ma) is based on the
208 produced AHe ages in our samples, according to the temperatures proposed by Shuster *et al.*
209 (2006). Constraint 'd' (30-10°C/10-0 Ma) is based on the fact that the collected samples
210 are currently at the surface. Constraint 'e' (300-10°C/300-170 Ma) helps the numerical
211 solution in finding acceptable and good paths. Moreover, it is based on the fact that prior to
212 deposition we lack geological evidences of the source provenance. Therefore, we cannot
213 define precise constraints. The large constraint 'e' allows the realisations to be at surface
214 as well as at buried temperatures before the deposition of the granitic boulder.

A. Parameters *AFT*

Annealing model – Ketcham *et al.*, 2007
C-axis projection – Ketcham *et al.*, 2007, 5.0M
Model c-axis projected lengths – yes
Default initial mean track length – From Dpar (μm)
Length reduction in standard – 0.893
Kinetic parameter – Dpar (μm)
Population number – one

Length Data

Goodness of fit method – Kuiper's Statistic

Age Data

Uncertainty mode – 1 SE (σ)

B. Parameters *He Apatite*

Model parameters

Calibration – Flowers *et al.*, 2009 (RDAAM Apatite)
Stopping distances – Ketcham *et al.*, 2011
Alpha calculation – Redistribution

Data

Age to report – Uncorrected (mean age)
Age alpha correction – Ketcham *et al.*, 2011

C. Inverse modeling

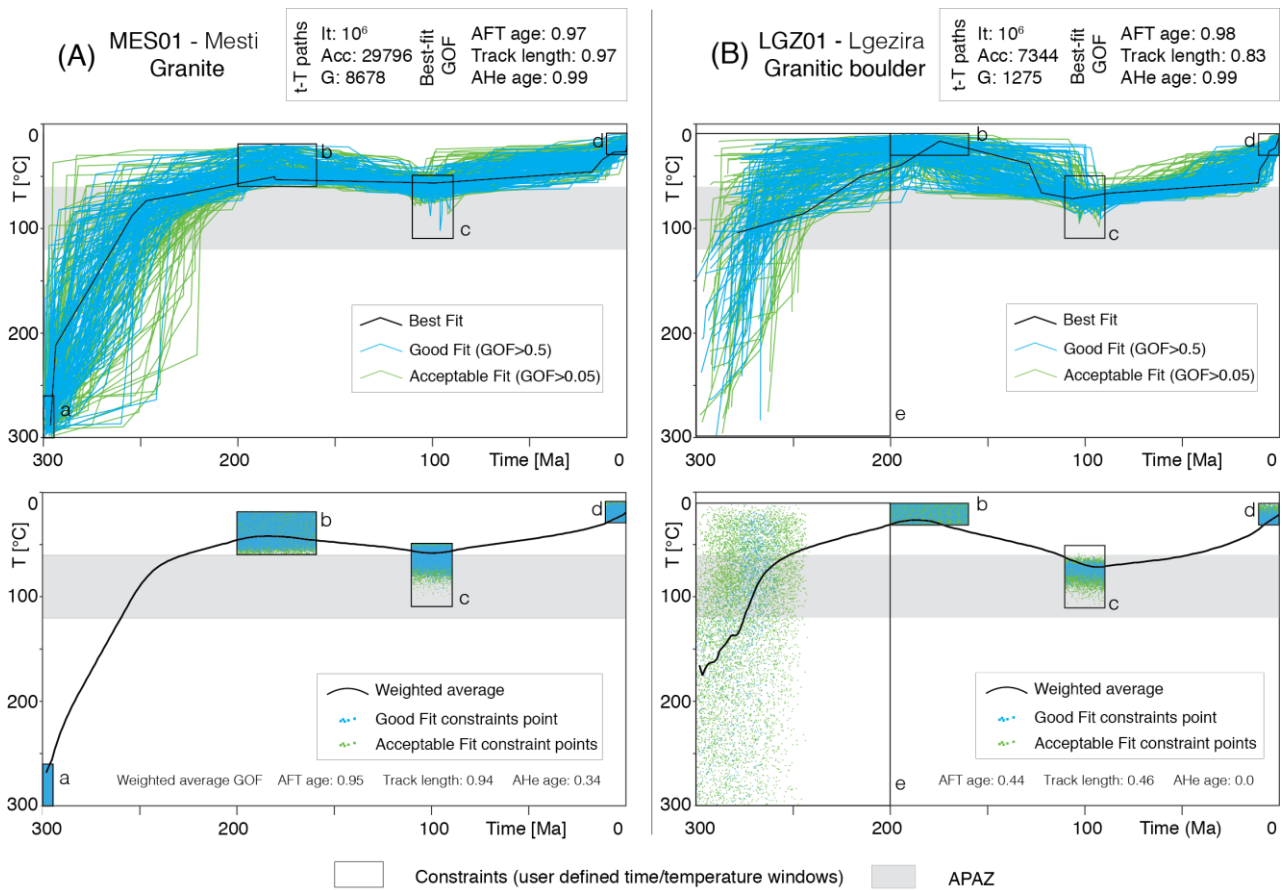
Search Method – Monte Carlo
Acceptable Path (GOF) - 0.05
Good Path (GOF) - 0.5
Subsegment spacing – Random
Ending condition – Path tried = 1000000

Segment parameters

Path between constraints - Monotonic consistent
Halve - 2 times
Randomizer style - Episodic
No imposed maximum dt/dt

215

216 Table 3. Input parameters used for both simulations, which are performed with the HeFTy
217 software (version 1.8.2; Apatite to Zircon; Ketcham, 2005). A) Parameters used for the AFT
218 models. Cf irradiation, see Donelick and Miller (1991); Dpar is the diameter of etched spontaneous
219 tracks measured parallel to the c-axis and is used as a proxy for the chemical composition of
220 apatite and therefore for the annealing properties (Donelick *et al.*, 1999); Kuiper's statistic, see
221 Press *et al.* (1992); SE stands for standard error. B) Parameters used for the AHe models. C)
222 Parameters used in the inverse modelling.



223

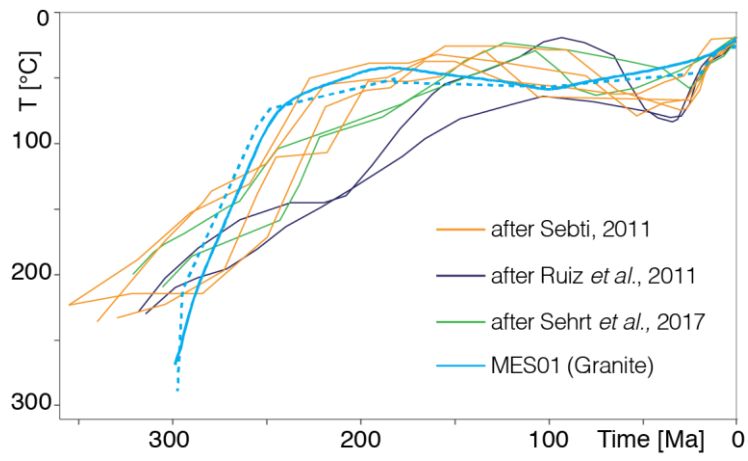
224 Figure 5. Results of t-T modelling for A) MES01 and B) LGZ01. Results are displayed with up
 225 to 200 curves for both good and acceptable goodness of fit (GOF) and the best-fit t-T path (upper
 226 panels) or with the constraint points and the weighted average (lower panels). Forward modelling
 227 was used to reproduce the weighted average curves in order to obtain their GOF values. See
 228 modelling parameters in table 3. It: number of iteration for the inverse modelling; Acc: acceptable
 229 paths; G: good paths. APAZ: Apatite Partial Annealing Zone.

230 The thermal modelling results are characterised by two cooling events, of significantly
231 different amplitudes, separated by a heating phase. Results for both samples are very
232 similar (fig. 5). The best-fit t-T path of MES01 shows a cooling event ending in the
233 Early/Middle Jurassic (cooling of $250\pm 10^{\circ}\text{C}$ between ca. 300 and 180 Ma), a subsequent
234 heating to temperatures of ca. $50\text{-}60^{\circ}\text{C}$ at the Early to Late Cretaceous boundary (heating
235 of ca. 10°C between ca. 180 and 100 Ma), followed by the second and last cooling
236 episode (cooling of ca. $30\pm 10^{\circ}\text{C}$ between 100 and 0 Ma). The timing of heating and
237 cooling episodes observed for the granitic boulder is similar, but this sample reached a
238 higher temperature (of ca. 70°C) during the heating episode. Between the two samples,
239 the weighted averages are nearly identical, with a Permian to Early/Middle Jurassic
240 cooling episode, Late Jurassic to Early Cretaceous heating episode, and Late Cretaceous
241 to present-day cooling episode. However, the two samples are characterised by different
242 temperature maxima and minima during each phase. At 170 Ma, temperatures are 20°C
243 cooler in the boulder, while the boulder reached temperatures ca. 10°C higher than the
244 granite sample at 100 Ma. We used the forward modelling option of HeFTy in order to
245 obtain the GOF of the weighted averages (fig. 5). While the AFT and AHe data of MES01
246 are reproduced, the GOF value of the LGZ01 AHe age is 0. When we increase the
247 temperatures of ca. 10°C at 95 Ma, the forwarded paths yield GOF values significantly
248 higher, especially with LGZ01, for which the AHe age GOF value reached 0.98. We
249 thereafter use the weighted average results to describe the evolution of the Sidi Ifni
250 transect, with 10°C added at ca. 95 Ma for LGZ01.

251

252 Previous LTT and t-T modelling studies carried-out in the Sidi Ifni area (figs. **2A** and **6**;
253 Sebti *et al.*, 2009; Sebti, 2011; Ruiz *et al.*, 2011; Sehrt *et al.*, 2017) concluded that a
254 Carboniferous-Early Cretaceous km-scale exhumation (8-6 km) was followed by a post-rift
255 subsidence (1-2 km) during the Late Cretaceous, and by an exhumation (2-2.5 km) during

256 the Cenozoic. Our best-fit results show similar trend and amplitudes as the previous
257 studies in the Sidi Ifni area (fig. 6 and references therein), with two cooling episodes
258 separated by a heating event; the timing, however, is significantly different. The main
259 reason lies in the age of the Mesozoic sediments used to constrain the curves, which were
260 assumed to be Early Cretaceous but have now been shown to be Middle Jurassic
261 (Arantegui *et al.*, 2016; see appendix). It is worth noting that three of the best-fit curves
262 from Sebti (2011) also show the post-Variscan exhumation ending during the Jurassic.
263 However, the related exhumation was interpreted as ending in the Early Cretaceous
264 because of all the other modelled t-T paths (good and acceptable realisations).



265

266 Figure 6. Best-fit (dashed) and weighted average t-T paths of MES01 compared to the best-fit
 267 t-T paths obtained in previous studies for samples of the Precambrian basement of the Sidi Ifni
 268 area.

269

5. Discussion

270

Post-Variscan evolution of the Sidi Ifni transect

271

Integrating results from LTT and t-T modelling with the backstripping of Ifni-1 well (Gouiza,

272

2011), we reconstructed the evolution of the Sidi Ifni transect (fig. 7). Following the

273

Variscan orogeny (fig. 7A), a major exhumation (ca. 7.5 km, using a geothermal gradient

274

of 25°C/km and a surface temperature of 20°C; e.g. Sehrt *et al.*, 2017) occurred in the

275

onshore domain during the Permian. This exhumation is also documented in the majority

276

of LTT studies conducted in the Anti-Atlas (e.g. Sebti *et al.*, 2009; Oukassou *et al.*, 2013).

277

Although offshore Permian sediments are undifferentiated from the base of the syn-rift

278

sediments, we consider the western part of the transect to have started subsiding during

279

the Permian.

280

During the Triassic and Early/Middle Jurassic, the upward movement of the eastern part of

281

the transect continued (ca. 1 km, using the above-mentioned geotherm), persisting until

282

ca. 180 Ma (fig. 7B). The exhumation ended either 15-10 Ma after the continental breakup

283

(Early Jurassic; ca. 195-190 Ma; Sahabi *et al.*, 2004; Labails *et al.*, 2010; Lundin and Doré,

284

2017) or 10 Ma before the continental breakup (Middle Jurassic; ca. 170; Klitgord *et al.*,

285

1986; Davison *et al.*, 2005; Gouiza *et al.*, 2010), as the onset of drifting in the Central

286

Atlantic is still debated. The related denudation event shed important volumes of

287

sediments to the west, as attested by the sediments accommodated by the SE dipping

288

normal faults (Le Roy and Piqué, 2001).

289

The unconformity recognised in the present day offshore domain between the Triassic and

290

the Middle Jurassic is correlated onshore to the unconformity between

291

Palaeozoic/Precambrian and Middle Jurassic sediments. We consider that the

292

Early/Middle Jurassic exhumation episode in the western Anti-Atlas affected also the

293

previously subsiding domain, reaching at least the vicinity of Ifni-1 well. Erosion affected

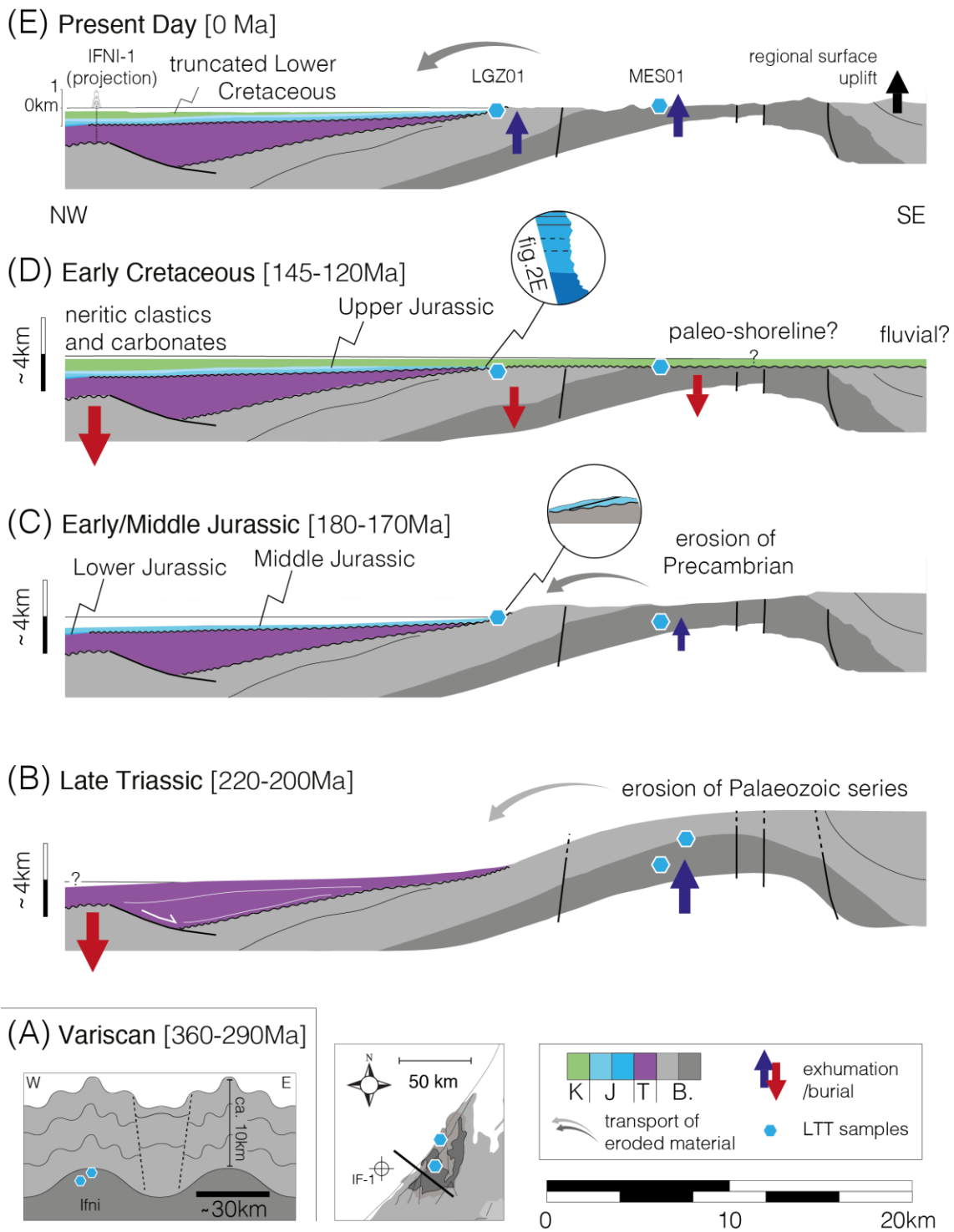
294

the Palaeozoic series and the Sidi Ifni granite (fig. 7C), until the exhumation ended in the

295 Early/Middle Jurassic. The sampled granitic boulder provenance may be the western Anti-
296 Atlas, as both samples share a similar t-T evolution.

297 During the Late Jurassic to Early Cretaceous (fig. **7D**), important subsidence occurred in
298 the offshore and onshore domains (between ca. 0.6 and 2 km). Related sediments are
299 characterised by neritic clastics and carbonates (Ifni-1) and by a fluvial dominated
300 environment (Sehrt *et al.*, 2017). This event is recorded in the Ifni-1 well by an acceleration
301 of the total subsidence rates, from ca. 0.02 to 0.03 km/Ma (Gouiza, 2011). A concomitant
302 subsidence episode is observed in the entire Anti-Atlas (Gouiza *et al.*, 2017).

303 Subsidence ends between the Early and Late Cretaceous at ca. 100 Ma and is followed by
304 exhumation from Late Cretaceous onwards (between ca. 1 and 2 km). The lack of Upper
305 Cretaceous sediments in the Ifni-1 well and up-dip truncations of the Lower Cretaceous
306 reflections indicate that the Late Cretaceous to Cenozoic exhumation reached the present-
307 day offshore domain (fig. **7E**) and that Lower Cretaceous sediments extended farther into
308 the western Anti-Atlas.



309

310 Figure 7. Conceptual model of the geological evolution of the Sidi Ifni transect; (E) is
 311 simplified from figure 3. Vertical movements estimated from t-T modelling results of MES01 and
 312 LGZ01 and backstripping of the Ifni-1 well (in Gouiza, 2011). The description of each stage is in the
 313 text. Horizontal scale is for B) to E) (no vertical exaggeration). B: undifferentiated basement
 314 offshore and Precambrian/Palaeozoic basement onshore; T: Triassic/Permian; J: Lower, Middle,
 315 and Upper Jurassic; K: Cretaceous. Thickness in the offshore domain is here estimated from Ifni-1
 316 well, hence no Early Jurassic at the well position was considered. Note that the granitic boulder
 317 has likely been sourced from the western Anti-Atlas as suggested in the text, and not necessarily
 318 from the Sidi Ifni granitic dome.

319 **Comparing the Sidi Ifni transect to other transects along the Moroccan rifted margin**

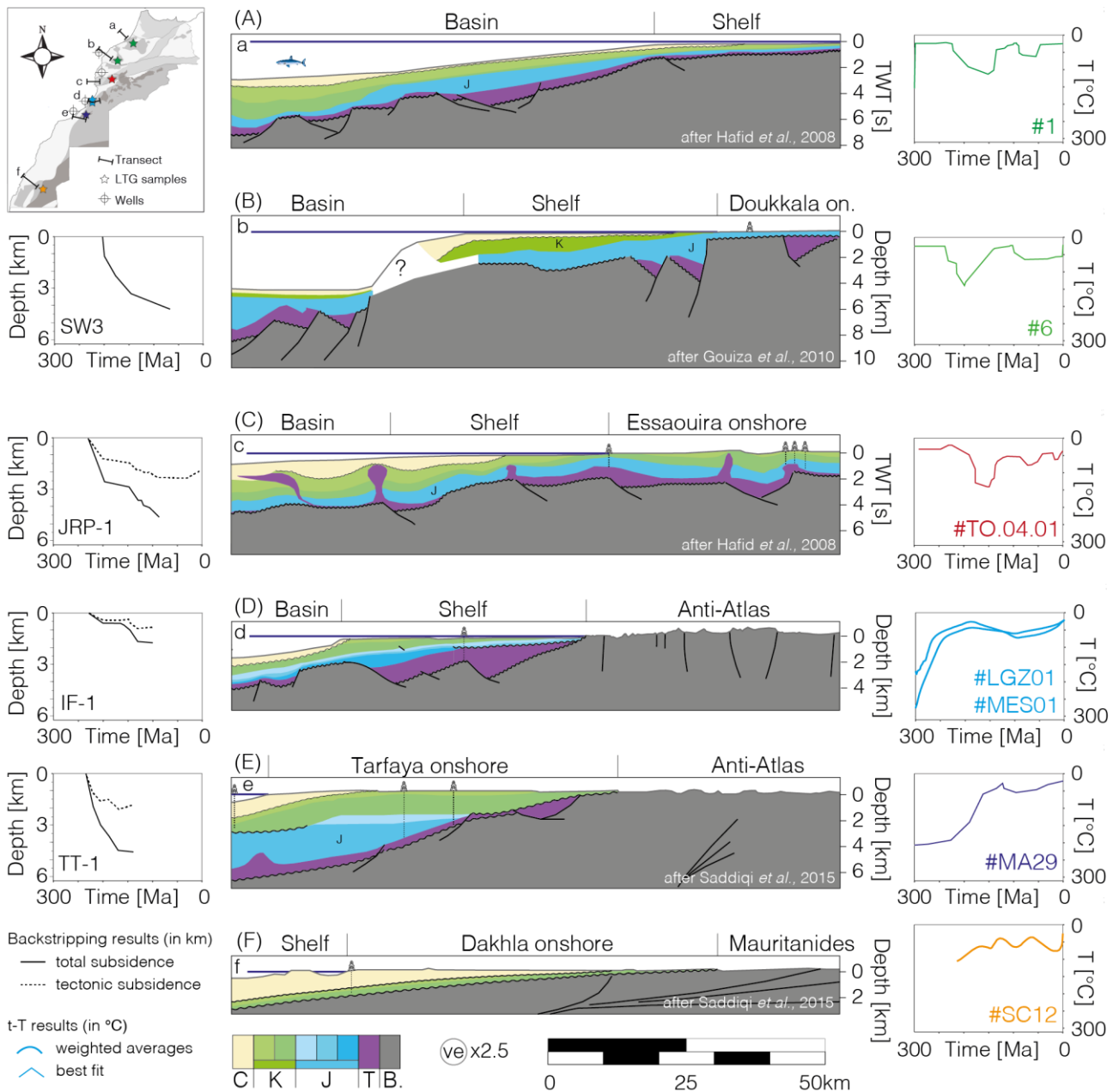
320 Five cross-sections perpendicular to the Moroccan rifted margin, across offshore and
321 onshore Atlantic basins are compared to the present-day Sidi Ifni transect (fig. **8**). To
322 compare the geological evolutions, we use published t-T models and subsidence curves
323 along these transects (fig. **8**).

324 The Doukkala, Rabat Offshore, and Essaouira transects (figs. **8A**, **B** and **C**, respectively)
325 all depict a Triassic or Jurassic unconformity over the basement, onshore as well as
326 offshore, and a relatively thick Mesozoic sedimentation (up to 2-3 km). The Upper
327 Cretaceous reflections are truncated at the present-day continental shelf edge (Hafid *et al.*,
328 2008), which is attributed to Cenozoic tectonics. In the Meseta and High Atlas, LTT studies
329 and t-T models have documented a similar kinematic evolution of vertical movements (e.g.
330 Ghorbal *et al.*, 2008; Domenech *et al.*, 2016). The presently outcropping Variscan rocks in
331 the Meseta were close to the surface during the Permian/Late Triassic, followed by
332 subsidence until the Middle Jurassic, exhumation in the Late Jurassic/Early Cretaceous,
333 renewed subsidence during the Late Cretaceous and a final exhumation in the Cenozoic.
334 Both Anti-Atlas sections (figs. **8D** and **E**) show a fairly thick Mesozoic package (between 2
335 and 5 km) at the western flank of the belt, with two to three unconformities: following the
336 Variscan folding, within the Jurassic and at the base of the Cenozoic. In the Anti-Atlas,
337 Gouiza *et al.* (2017) and this study document a similar thermal evolution, although different
338 from the one described in the Meseta (e.g. Ghorbal *et al.*, 2008).

339 The differences in post-Variscan thermal evolutions of the Meseta/High Atlas and Anti-
340 Atlas highlight several shifts of source areas for the sediments delivered to the Atlantic and
341 coastal basins between the Middle and Late Jurassic and between the Early and Late
342 Cretaceous.

343 Finally, the Dakhla section (fig. **8F**) shows that no sediments are preserved prior to the
344 Early Cretaceous (Ranke *et al.*, 1982; Saddiqi *et al.*, 2015) west of the Mauritanides/
345 Reguibat Shield. The thickness of the Cretaceous deposits may have reached 2 km,

346 unconformably overlain by Palaeocene sediments (Ranke *et al.*, 1982). The documented
347 kinematic evolution (e.g. Leprêtre *et al.* 2015) is also different from those of other
348 segments, showing subsidence from the Permian to the Triassic and exhumation from
349 Jurassic onwards for most of the Reguibat Shield, with locally shorter and milder
350 exhumation and subsidence episodes (e.g. Leprêtre *et al.*, 2015).



351

352 Figure 8. Present-day 2D architecture of the Moroccan passive margin (central panels),
 353 selected subsidence and backstripping curves (left panels), and t-T modelling (right panels) results.
 354 Note that cross-sections a and c are in time. See location map for orientation. C: Cenozoic; same
 355 stratigraphy legend as figure 7. The letters “J” and “K” are shown on the sections if the Jurassic or
 356 Cretaceous are locally undifferentiated. The t-T best-fit results of samples 1/6, TO.04.01 and MA29
 357 are from Ghorbal *et al.*, 2008, Ghorbal, 2009 and Sehrt *et al.*, 2017, respectively. The t-T weighted
 358 average results of samples LGZ01/MES01 and SC12 are from the present work and Leprière
 359 *et al.*, 2015, respectively. The subsidence curves from wells SW3 (synthetic), JRP-1 and IF-1/TT-1
 360 are from Gouiza *et al.*, 2010, Bouatmani *et al.*, 2007 and Gouiza, 2011, respectively.

361 **Vertical movements mechanisms**

362 The pre-rift exhumation is a result of the erosion following the Variscan orogeny (post-
363 orogeny collapse), while the mechanisms responsible for the syn- and early post-rift
364 exhumation remain unconstrained. The observed syn-rift exhumation is not linked to rift
365 shoulder uplift, as proposed for the Anti-Atlas by previous authors (e.g. Oukassou *et al.*,
366 2013; Soulaïmani *et al.*, 2014), for two reasons: (1) the Permian to Jurassic exhumation
367 started before the initiation of rifting and (2) Late Triassic sediments are well represented
368 east of the Atlantic faults (offshore Sidi Ifni). However, we do not discard a surface uplift as
369 the majority of t-T models in the Anti-Atlas document an exhumation during the Central
370 Atlantic syn-rift period.

371 The post-rift burial shown in the evolution of the Sidi Ifni transect is a results of the large
372 scale denudation of areas in the north (Meseta/Western High Atlas; e.g. Bertotti and
373 Gouiza, 2012) and in the south (Reguibat Shield; e.g. Leprêtre *et al.*, 2015), routing
374 sediments over the Anti-Atlas and towards the offshore. The Late Cretaceous exhumation
375 may be explained by crustal horizontal stresses propagating following the onset of the
376 South Atlantic drift (e.g. Michard *et al.*, 2008a; Ghorbal *et al.*, 2008).

377

6. Conclusions

378 The t-T modelling results constrained by Middle Jurassic stratigraphy preserved along the
379 coast allowed the reconstruction of the geological evolution of the Sidi Ifni transect.
380 Results indicate the exhumation of the onshore domain of the transect by ca. 7.5 km
381 between the end of the Variscan orogeny and the Early/Middle Jurassic. Erosion affected
382 the Palaeozoic series and eventually reached the Precambrian basement. Eroded material
383 was routed to the subsiding Mesozoic basin to the northwest. Rocks along the transect
384 were subsequently buried to a depth of 0.6 to 2 km during the Late Jurassic and the Early
385 Cretaceous. The burial event is documented in the offshore well (IF-1) by an acceleration
386 of the total subsidence rates. From late Early/Late Cretaceous onwards, the transect rocks
387 were exhumed by 1 to 2 km onshore, while the Lower Cretaceous deposits in the
388 continental shelf were exposed and eroded (truncated reflections).

389 The comparison of the Sidi Ifni transect to other transects along the rifted margin of
390 Morocco highlights changes in the architecture of the offshore Mesozoic deposit. We show
391 here that the above defined segments along the margin underwent significantly different
392 kinematic evolutions, with specific vertical movement patterns in the hinterland and basins.

393 The comparison of the t-T models of the Meseta/High Atlas to the Anti-Atlas shows two
394 major shifts in the active sediment source areas during the Jurassic and Cretaceous
395 periods.

Acknowledgments

396
397 The authors, all NARG members (North Africa Research Group), thank the ONHYM
398 (Office National des Hydrocarbures et des Mines) for field work support and access to
399 internal reports. We are thankful to B.Louis, I.Coutand, and R.Kislitsyn of Dalhousie
400 University (Halifax, Canada) for the produced radiometric ages. M.Gouiza (Leeds, UK) is
401 thanked for providing extra material used in this work.
402 M.Simmons (NHM, London), B.Granier (Brest, France), R.Gatto and S.Monari (Padua,
403 Italy) are thanked for their work on the palaeontology data presented in the appendix.
404 We thank M.Gouiza and an anonymous reviewer for their constructive comments that
405 significantly helped to improve the present work.

Funding

406
407 This work was supported by the Integrated for Solid Earth Sciences (ISES; PhD project
408 funding of the first author) and by the North Africa Research Group (NARG).

- Amidon**, W.H., Roden-Tice, M., Anderson, A.J., McKeon, R.E. and Shuster, D.L., 2016. Late Cretaceous unroofing of the White Mountains, New Hampshire, USA: An episode of passive margin rejuvenation?: *Geology*, **44**, 415–418.
- Arantegui**, A., Lubert, T., Charton, R., Simmons, M., Bertotti, G. and Redfern, J., 2016. Temporal and spatial evolution of Mesozoic drainage systems feeding the deepwater Atlantic passive margin of Morocco: Tarfaya Basin: *Conference Abstract, 32nd Meeting of Sedimentology, IAS Marrakech*, 1–2.
- Bertotti**, G. and Gouiza, M., 2012. Post-rift vertical movements and horizontal deformations in the eastern margin of the Central Atlantic: Middle Jurassic to Early Cretaceous evolution of Morocco: *International Journal of Earth Sciences*, **101**, 2151–2165.
- Bigot-Cormier**, F., 2002. La surrection du massif cristallin externe de l'Argentera (France-Italie) et ses relations avec la déformation pliocène de la marge Nord-Ligure : Arguments thermo-chronologiques (traces de fission), géomorpho-logiques et interprétations de sismique marine: *PhD Thesis, Université Nice Sophia Antipolis*, 354 pp.
- Bouatmani**, R., Chakor Alami, A. and Medina, F., 2007. Subsidence, évolution thermique et maturation des hydrocarbures dans le bassin d'Essaouira (Maroc): apport de la modélisation: *Bulletin Institut Scientifique-Rabat*, **29**, 15–36.
- Burkhard**, M., Caritg, S., Helg, U., Robert-Charrue, C. and Soulaymani, A., 2006. Tectonics of the Anti-Atlas of Morocco: *Comptes Rendus Geoscience*, **338**, 11–24.
- Choubert**, G., Faure-Muret, A. and Hottinger, L., 1966. Aperçu Géologique du Bassin Cotier de Tarfaya. In : *Le Bassin Cotier de Tarfaya (Maroc meridional), Tome I, Stratigraphie*, Notes et Memoires du Service Geologique, **115**, 7-222.

- Davison, I.**, 2005, Central Atlantic margin basins of North West Africa: Geology and hydrocarbon potential (Morocco to Guinea): *Journal of African Earth Sciences*, **43**, 254–274.
- Domènech, M.**, Teixell, A., Babault, J. and Arboleya, M.-L., 2015. The inverted Triassic rift of the Marrakech High Atlas: A reappraisal of basin geometries and faulting histories: *Tectonophysics*, **663**, 177–191.
- Donelick, R.A.** and Miller, D.S., 1991. Enhanced TINT fission track densities in low spontaneous track density apatites using ²⁵²Cf-derived fission fragment tracks: A model and experimental observations: *Nuclear Tracks and Radiation Measurements*, **18**, 301–307.
- Donelick, R.A.**, Ketcham, R.A. and Carlson, W.D., 1999. Variability of apatite fission-track annealing kinetics II. Crystallographic orientation effects: *American Mineralogist*, **84**, 1224–1234.
- Farley, K.A.**, 2002. (U-Th)/He Dating: Techniques, Calibrations, and Applications: *Reviews in Mineralogy and Geochemistry*, **47**, 819–844.
- Fleischer, R.L.** and Hart, H.R., 1972. Fission track dating: techniques and problems. *Calibration of Hominoid Evolution*, **135**, 170.
- Flowers, R.M.**, Ketcham, R.A., Shuster, D.L. and Farley, K.A., 2009. Apatite (U–Th)/He thermochronometry using a radiation damage accumulation and annealing model: *Geochimica et Cosmochimica Acta*, **73**, 2347–2365.
- Frizon de Lamotte, D.**, Leturmy, P., Missenard, Y., Khomsi, S., Ruiz, G., Saddiqi, O., Guillocheau, F. and Michard, A., 2009. Mesozoic and Cenozoic vertical movements in the Atlas system (Algeria, Morocco, Tunisia): An overview: *Tectonophysics*, **475**, 9–28.
- Fuller, J.**, Fernández, M., Zeyen, H. and Vergés, J., 2007. A rapid method to map the crustal and lithospheric thickness using elevation, geoid anomaly and thermal analysis.

Application to the Gibraltar Arc System, Atlas Mountains and adjacent zones:

Tectonophysics, **430**, 97–117.

Gallagher, K., Brown, R. and Johnson, C., 1998. Fission track analysis and its applications to geological problems: *Annual Review of Earth and Planetary Sciences*, **26**, 519–572.

Ghorbal, B., Bertotti, G., Foeken, J. and Andriessen, P., 2008. Unexpected Jurassic to Neogene vertical movements in 'stable' parts of NW Africa revealed by low temperature geochronology: *Terra Nova*, **20**, 355–363.

Ghorbal, B., 2009. Mesozoic to Quaternary thermo-tectonic evolution of Morocco (NW Africa): *PhD Thesis, Vrije Universiteit Amsterdam*, 231 pp.

Gouiza, M., 2011. Mesozoic source-to-sink systems in NW Africa: Geology of vertical movements during the birth and growth of the Moroccan rifted margin: *PhD Thesis, Vrije Universiteit Amsterdam*, 192 pp.

Gouiza, M., Bertotti, G., Hafid, M. and Cloetingh, S., 2010. Kinematic and thermal evolution of the Moroccan rifted continental margin: Doukkala-High Atlas transect: *Tectonics*, **29**, 1-22.

Gouiza, M., Charton, R., Bertotti, G., Andriessen, P. and Storms, J.E.A., 2017. Post-Variscan evolution of the Anti-Atlas belt of Morocco constrained from low-temperature geochronology: *International Journal of Earth Sciences*, **106**, 593–616.

Hafid, M., Tari, G., Bouhadioui, I., Moussaid, El, E., Echarfaoui, H., Aït Salem, H., Nahim, M. and Dakki, M., 2008. Atlantic Basins. In: *Continental Evolution: The Geology of Morocco*, Springer Science & Business Media.

Helg, U., Burkhard, M., Caritg, S. and Robert-Charrue, C., 2004. Folding and inversion tectonics in the Anti-Atlas of Morocco: *Tectonics*, **23**, TC4006.

- Hollard**, H., Choubert, G., Bronner, G., Marchand, J. and SOUGY, J., 1985. Carte Géologique du Maroc, scale 1/1000000 (2 sheets): *Notes et Mémoires du Service Géologique du Maroc*, **260**.
- Hurford**, A.J., 1990. Standardization of Fission Track Dating Calibration: Recommendation by the Fission Track Working Group of the I.O.G.S. Subcommittee on Geochronology: *Chemical Geology*, **80**, 171–178.
- Japsen**, P., Bonow, J.M., Green, P.F., Chalmers, J.A. and Lidmar-Bergström, K., 2006. Elevated, passive continental margins: Long-term highs or Neogene uplifts? New evidence from West Greenland: *Earth and Planetary Science Letters*, **248**, 330–339.
- Japsen**, P., Green, P.F., Bonow, J.M., Hinchey, A.M. and Wilton, H.C., 2016. Burial and exhumation history of the Labrador- Newfoundland margin: first observations: *Geologic survey of Denmark and Greenland bulletin*, **35**, 91-94.
- Jelinek**, A.R., Chemale, F., Jr, van der Beek, P.A., Guadagnin, F., Cupertino, J.A. and Viana, A., 2014. Denudation history and landscape evolution of the northern East-Brazilian continental margin from apatite fission-track thermochronology : *Journal of South American Earth Sciences*, **54**, 158–181.
- Ketcham**, R.A., 2005. Forward and Inverse Modeling of Low-Temperature Thermochronometry Data: *Reviews in Mineralogy and Geochemistry*, **58**, 275–314.
- Ketcham**, R.A., Carter, A., Donelick, R.A., Barbarand, J. and Hurford, A.J., 2007. Improved modeling of fission-track annealing in apatite: *American Mineralogist*, **92**, 799–810.
- Ketcham**, R.A., Gautheron, C. and Tassan-Got, L., 2011. Accounting for long alpha-particle stopping distances in (U-Th-Sm)/He geochronology: Refinement of the baseline case: *Geochimica et Cosmochimica Acta*, **75**, 7779–7791.

- Klitgord**, K.D., Schouten, H., Vogt, P.R. and Tucholke, B.E., 1986. Plate kinematics of the Central Atlantic. In: *The Western North Atlantic Region: The Geology of North America*, Geological Society of America.
- Labails**, C., Olivet, J.-L., Aslanian, D. and Roest, W.R., 2010. An alternative early opening scenario for the Central Atlantic Ocean: *Earth and Planetary Science Letters*, **297**, 355–368.
- Le Roy**, P. and Piqué, A., 2001. Triassic-Liassic Western Moroccan synrift basins in relation to the Central Atlantic opening: *Marine Geology*, **172**, 359–381.
- Leprêtre**, R., Missenard, Y., Barbarand, J., Gautheron, C., Saddiqi, O. and Pinna-Jamme, R., 2015. Post-rift history of the eastern Central Atlantic passive margin: insights from the Saharan region of South Morocco: *American Geophysical Union*, 1–58.
- Louis**, B., 2015. Late Cenozoic Upper-Crustal Cooling History of the Shuswap Metamorphic Complex, Southern Canadian Cordillera, British Columbia: New Insights From Low-Temperature Multi- Thermochronometry and Inverse Thermal Modeling: *MSc Thesis, Dalhousie University*, 226 pp.
- Lundin**, E.R. and Doré, A.G., 2017. The Gulf of Mexico and Canada Basin: Genetic Siblings on Either Side of North America: *GSA Today*, **27**, 4–11.
- Martinis**, B. and Visintin, V., 1966. Données géologiques sur le bassin sédimentaire côtier de Tarfaya (Maroc méridional): *Bassins sédimentaires du Littoral africain*, In: *Bassins sédimentaires du littoral africain*. Association des Services Géologiques Africain.
- Michard**, A., Saddiqi, O., Chalouan, A. and Frizon de Lamotte, D., 2008a. Continental Evolution: *Continental Evolution: The Geology of Morocco*. Springer Science & Business Media, 426 pp.
- Michard**, A., Hoepffner, C., Soulaïmani, A. and Baidder, L., 2008b. The Variscan Belt. In: *Continental Evolution: The Geology of Morocco*. Springer Science & Business Media.

- Oukassou**, M., Saddiqi, O., Barbarand, J., Sebti, S., Baidder, L. and Michard, A., 2013. Post-Variscan exhumation of the Central Anti-Atlas (Morocco) constrained by zircon and apatite fission-track thermochronology: *Terra Nova*, **25**, 151–159.
- Piqué**, A., Tricart, P., Guiraud, R., Laville, E., Bouaziz, S., Amrhar M. and Ouali, R.A., 2002. The Mesozoic-Cenozoic Atlas belt (North Africa): an overview: *Geodinamica Acta*, **15**, 185–208.
- Press**, W.H., Flannery, B.P., Teukolsky, S.A. and Vetterling, W.T., 1992. *Numerical Recipes in FORTRAN 77: Volume 1, Fortran Numerical Recipes*. Cambridge University Press.
- Ranke**, U., von Rad, U., & Wissmann, G., 1982. Stratigraphy, facies and tectonic development of the on-and offshore Aaiun-Tarfaya Basin—A review. In: *Geology of the Northwest African continental margin*. Springer Berlin Heidelberg.
- Rougier**, S., Missenard, Y., Gautheron, C., Barbarand, J., Zeyen, H., Pinna, R., Liégeois, J.-P., Bonin, B., Ouabadi, A., El-Messaoud Derder, M., Frizon de Lamotte, D., 2013. Eocene exhumation of the Tuareg Shield (Sahara Desert, Africa): *Geology*, **41**, 615–618.
- Ruiz**, G.M., Helg, U., Negro, F., Adatte, T. and Burkhard, M., 2008. Illite crystallinity patterns in the Anti-Atlas of Morocco: *Swiss Journal of Geosciences*, **101**, 387–395.
- Ruiz**, G.M.H., Sebti, S., Negro, F., Saddiqi, O., Frizon de Lamotte, D., Stockli, D., Foeken, J., Stuart, F., Barbarand, J. and Schaer, J.P., 2011. From central Atlantic continental rift to Neogene uplift - western Anti-Atlas (Morocco): *Terra Nova*, **23**, 35–41.
- Saddiqi**, O., Rjimati, E., Michard, A., Soulaïmani, A. and Ouanaimi, H., 2015. Recommended Geoheritage Trails in Southern Morocco: A 3 Ga Record Between the Sahara Desert and the Atlantic Ocean. In: *From Geoheritage to Geoparks, Geoheritage, Geoparks and Geotourism*. Springer International Publishing.
- Sahabi**, M., Aslanian, D. and Olivet, J. L., 2004. A new starting point for the history of the central Atlantic: *Comptes Rendus Geoscience*, **336**, 1041–1052.

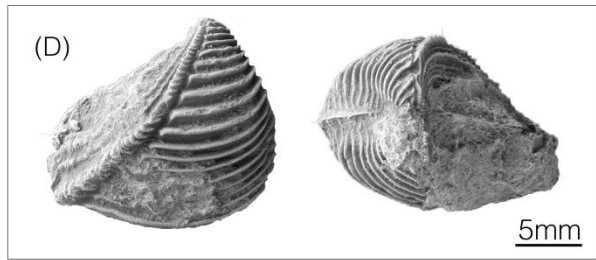
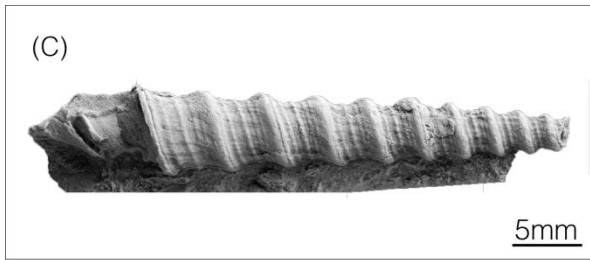
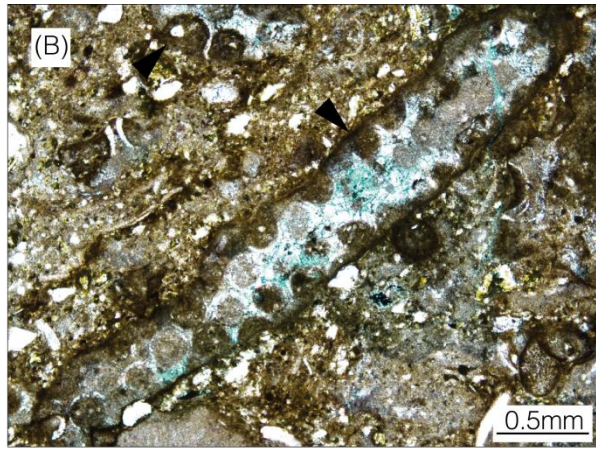
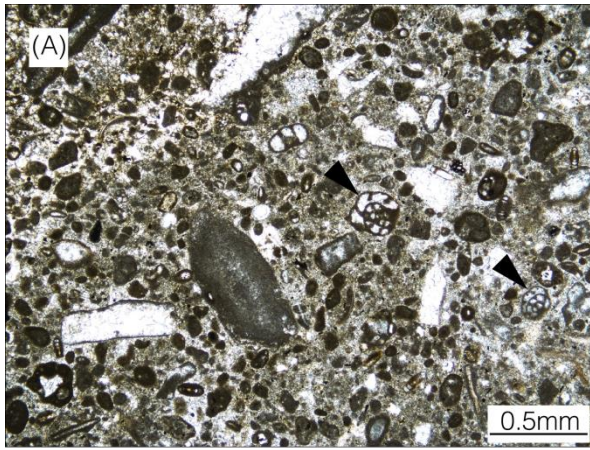
- Sebti**, S., 2011. Mouvements verticaux de l'Anti-Atlas occidental Marocain (Kerdous & Ifni): Thermochronologie par traces de fission: *PhD Thesis, Université Hassan II Casablanca*, 173 pp.
- Sebti**, S., Saddiqi, O., Haimmer, El, F.-Z., Michard, A., Ruiz, G., Bousquet, R., Baidder, L. and Frizon de Lamotte, D., 2009. Vertical movements at the fringe of the West African Craton: First zircon fission track datings from the Anti-Atlas Precambrian basement, Morocco: *Comptes Rendus Geoscience*, **341**, 71–77.
- Sehrt**, M., Glasmacher, U. A., Stockli, D. F., Jabour, H., and Kluth, O., 2017. The southern Moroccan passive continental margin: An example of differentiated long-term landscape evolution in Gondwana: *Gondwana Research*, In Press.
- Shuster**, D.L., Flowers, R.M. and Farley, K.A., 2006. The influence of natural radiation damage on helium diffusion kinetics in apatite: *Earth and Planetary Science Letters*, **249**, 148–161.
- Soulaimani**, A., Michard, A., Ouanaimi, H., Baidder, L., Raddi, Y., Saddiqi, O. and Rjimati, E.C., 2014. Late Ediacaran–Cambrian structures and their reactivation during the Variscan and Alpine cycles in the Anti-Atlas (Morocco): *Journal of African Earth Sciences*, **98**, 94–112.
- Tassone**, D.R., Holford, S.P., Hillis, R.R. and Tuitt, A.K., 2012. Quantifying Neogene plate-boundary controlled uplift and deformation of the southern Australian margin: *Geological Society, London, Special Publications*, **367**, 91–110.
- Thomas**, R.J., Fekkak, A., Ennih, N., Errami, E., Loughlin, S.C., Gresse, P.G., Chevallier, L.P. and Liégeois, J.P., 2004. A new lithostratigraphic framework for the Anti-Atlas Orogen, Morocco: *Journal of African Earth Sciences*, **39**, 217–226.
- Vermeesch**, P., 2009. RadialPlotter: A Java application for fission track, luminescence and other radial plots: *Radiation Measurements*, **44**, 409–410.

- Watts**, A.B., 2012. Models for the evolution of passive margins. In: *Regional Geology and Tectonics: Phanerozoic Rift Systems and Sedimentary Basins*. Elsevier, Amsterdam.
- Wildman**, M., Brown, R., Watkins, R., Carter, A., Gleadow, A. and Summerfield, M., 2015. Post break-up tectonic inversion across the southwestern cape of South Africa: New insights from apatite and zircon fission track thermochronometry: *Tectonophysics*, **654**, 30–55.
- Yamato**, P., Husson, L., Becker, T.W. and Pedoja, K., 2013. Passive margins getting squeezed in the mantle convection vice: *Tectonics*, **32**, 1559–1570.
- Yazidi**, A., Benziane, F., Hassenforder, B., Destombes, J., Hollard, H., Bourgin, R. and Oliva, P., 1991. Carte Géologique du Maroc: Tiznit, scale 1/100000: *Notes et Mémoires du Service Géologique du Maroc*, **360**.
- Yazidi**, A., Benziane, F., Hollard, H., Oliva, P. and Destombes, J., 1986. Carte Géologique du Maroc and Notice: Sidi Ifni, scale 1/100000: *Notes et Mémoires du Service Géologique du Maroc*, **310**.

Appendix

The sediments exposed along Craima Beach were mapped by Yazidi *et al.* (1986) as Lower to Middle Cretaceous red sandstones with conglomerate interbeds, bituminous marls and limestones with *Natica* and *Ampulina* of Sidi Ouarzik, overlying red conglomerates. The age was originally established on poorly preserved ostracods. A detailed study of the faunal content of the succession is in progress (Arantegui *et al.*, in prep.). The micro- and macro-palaeontology analysis show that the assemblage of benthic foraminifera (fig. **A**) [*Nautiloculina oolithica* (Möhler)], green algae (fig. **B**) [*Holosporella siamensis* (Pia)], nerinids gastropods (fig. **C**) [*Nerinella elegantula* (d'Orbigny), *Ampullospira actaea* (d'Orbigny), and *Ceritella dewalquei* (Piette)] and trigoniids bivalves (fig. **D**) [*Trigonia pullus* (J. de C. Sowerby)] unequivocally indicates a Middle Jurassic age by comparison with the known occurrence of its components in western Europe (Fischer, 1969; Elliott, 1983; Bassoulet, 1987; Kuss, 1990; Fischer and Weber, 1997; Holzapfel, 1998).

In the north of the present study outcrops are mapped as Lower Cretaceous red conglomerates, sandstones and grey and pink argillaceous sandstones overlain by Middle Cretaceous dolomites, limestones and marly limestones with trigoniids, alectryonids and nerineids (Yazidi *et al.*, 1991). The great resemblance in facies and fauna with the study area of Arantegui *et al.* (in prep.) strongly suggests a generalized misdating of the Mesozoic outcrops in the Sidi Ifni area.



Micro- and macro-fauna from the Middle Jurassic assemblage in the limestones of Craima beach. A) *Nautiloculina oolithica*, B) *Holosporella siamensis*, C) *Nerinella eleganta*, and D) *Trigonia pullus*.

Appendix References

- Arantegui et al.**, in prep.. New data from the eastern margin of the Central Atlantic constraining early Mesozoic and post-rift evolution and depositional systems (provisional title).
- Fischer**, J.-C., 1969. Géologie, paléontologie et paléoécologie du Bathonien en sud-ouest du Massiv Ardennais: *Mémoires du Muséum National d'Histoire naturelle de Paris*, **20**, 319pp.
- Fischer**, J.-C. and Weber, C., 1997. Révision critique de la Paléontologie Française d'Alsace d'Orbigny (incluant la réédition de l'original). Volume II, gastropodes jurassiques: *Muséum National d'Histoire Naturelle de Paris*, **2**, 300pp.
- Holzappel**, S., 1998. Palökologie benthischer Faunengemeinschaften und Taxonomie der Bivalven im Jura von Südtunesien: *Beringeria*, **22**, 3–119.
- Yazidi**, A., Benziane, F., Hassenforder, B., Destombes, J., Hollard, H., Bourgin, R. and Oliva, P., 1991. Carte Géologique du Maroc: Tiznit, scale 1/100000: *Notes et Mémoires du Service Géologique du Maroc*, **360**, 1pp.
- Yazidi**, A., Benziane, F., Hollard, H., Oliva, P. and Destombes, J., 1986. Carte Géologique du Maroc and Notice: Sidi Ifni, scale 1/100000: *Notes et Mémoires du Service Géologique du Maroc*, **310**, 1pp.
- Bassoulet**, J.-P. 1987. *Sarfatiella dubari* Conrad & Peybernès 1973: a junior synonym of *Holosporella siamensis* Pia 1930 : *4th International Symposium on Fossil Algae*, Friends of the Algae Newsletter, 20–21.
- Elliott**, G.F. 1983. Distribution and affinities of the Jurassic dasycladalean alga *Sarfatiella*: *Palaeontology*, **26**, 671–675.
- Kuss**, J. 1990. Middle Jurassic Calcareous Algae from the Circum-Arabian Area: *Facies*, **22**, 59–85.

Kuznetsova, K.K., Grigelis, A., Adjamian, J. and Hallaq, L. 1996. Zonal stratigraphy and foraminifera of the Tethyan Jurassic (Eastern Mediterranean): *Gordon and Breach Publishers*, 256pp.